Bioorganic & Medicinal Chemistry 19 (2011) 1321–1327

Contents lists available at ScienceDirect

Bioorganic & Medicinal Chemistry

journal homepage: www.elsevier.com/locate/bmc

Synthesis and evaluation of phosphonated *N*-heteroarylcarboxamides as DOXP-reductoisomerase (DXR) inhibitors

Taryn Bodill [c], Anne C. Conibear [a], Gregory L. Blatch [b,c], Kevin A. Lobb [a,c], Perry T. Kaye [a,c,*]

[a] Department of Chemistry, Rhodes University, Grahamstown 6140, South Africa
[b] Biomedical Biotechnology Research Unit and Department of Biochemistry, Rhodes University, Grahamstown 6140, South Africa
[c] Centre for Chemico- and Biomedicinal Research, Rhodes University, Grahamstown 6140, South Africa

ARTICLE INFO

Article history:
Received 22 September 2010
Revised 22 November 2010
Accepted 25 November 2010
Available online 2 December 2010

Keywords:
Anti-malarial
Phosphonates
DOXP-reductoisomerase
Enzyme inhibitors
In silico docking
Saturation Transfer Difference NMR

ABSTRACT

The diethyl esters and disodium salts of a range of heteroarylcarbamoylphosphonic acids have been prepared and evaluated as analogues of the highly active DOXP-reductoisomerase (DXR) inhibitor, fosmidomycin. Computer-simulated docking studies, Saturation Transfer Difference (STD) NMR analysis and enzyme inhibition assays have been used to explore enzyme-binding and -inhibition potential, while in silico analysis of the DXR active site has highlighted the importance of including a well-parameterised metal co-factor in docking studies and has revealed the availability of an additional binding pocket to guide future drug design.

1. Introduction

Malaria continues to be an enormous health-threat in the developing world. Treatment is compounded by the phenomenon of drug resistance, and the development of novel therapeutics has become a research priority.[1–3] *Plasmodium falciparum* (*Pf*) is the parasite responsible for the most dangerous form of human malaria, and the enzyme, 1-deoxy-1-D-xylulose 5-phosphate (**1**; Fig. 1) reductoisomerase (*Pf*DXR) has recently been validated as a target for the design of potential antimalarial drugs.[4,5] This enzyme is involved in a parasite-specific, isoprenoid biosynthetic DOXP/MEP pathway, for which the natural product, fosmidomycin **2**,[6,7] and its acetyl analogue, FR900098 **3**,[6,7] have been shown to act as inhibitors. Fosmidomycin **2** was isolated from *Streptomyces lavendulae* in the 1970s and found to have antibiotic and herbicidal properties.[5,6,8,9] The DOXP/MEP pathway has also been found in several pathogenic species such as *Helicobacter pylori, Mycobacterium tuberculosis*, *Escherichia coli (Ec)* and *P. falciparum* but, since it is not found in humans, it has obvious potential as a target for chemotherapy.[8] In humans, fosmidomycin **2** has been shown to be active against uncomplicated *P. falciparum* malaria, but its efficacy as a clinical drug is compromised by poor absorption, short plasma half-life and the high observed rate of recrudescence.[7,8] Nevertheless, the high levels of DXR inhibition exhibited by fosmidomycin **2** and FR900098 **3** have made these compounds particularly promising leads for the development of novel and effective antimalarials.[7] Although few of the DXR inhibitors described in the literature have been more effective than fosmidomycin, they provide useful structure–activity relationships to guide the design of new inhibitors. Deng et al. have highlighted the importance of a metal-coordinating group, especially nitrogen- and oxygen-containing functionalities which are able to bind to the hard Mg^{2+} ion.[10] The phosphonate moiety of fosmidomycin **2** is more biologically stable than the corresponding phosphate of DOXP **1** and the importance of the double negative charge on the phosphonate group has also been demonstrated.[11,12]

In our laboratories, attention has been given to designing and synthesising fosmidomycin **2** analogues as potential DXR inhibitors, and we have recently reported[9] the synthesis of a series of phosphonated *N*-phenylcarboxamides **4**. We now describe: (i) the preparation of novel *N*-heteroarylamino-2-oxoethylphosphonate esters **8a–e** and the disodium salts **11a–e** of the corresponding phosphonic acids **9a–e** (Scheme 1); (ii) the use of *Ec*DXR in STD NMR ligand-binding and enzyme inhibition studies; (iii) the results of in silico ligand-docking studies; and (iv) progress in the topological analysis of the enzyme active site.

2. Results and discussion

2.1. Chemistry

Deng et al.[10] have highlighted the role of metal-coordinating groups (especially nitrogen- or oxygen-containing functionalities)

* Corresponding author. Tel.: +27 46 6037030; fax: +27 46 6225109.
E-mail address: P.Kaye@ru.ac.za (P.T. Kaye).

0968-0896/$ - see front matter © 2010 Elsevier Ltd. All rights reserved.
doi:10.1016/j.bmc.2010.11.062

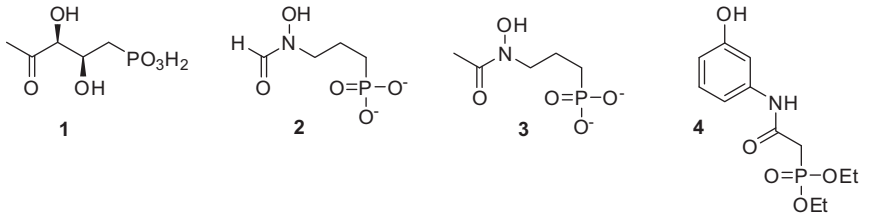

Figure 1. Structures of DOXP **1** and known and putative DXR inhibitors **2–4**.

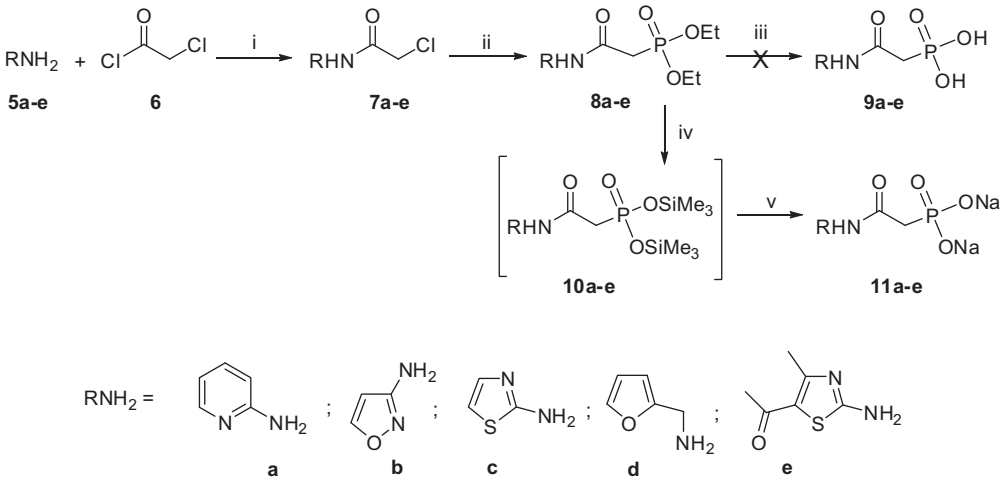

Scheme 1. Synthesis of phosphonate esters **8a–e** and phosphonic acid salts **11a–e**. Reagents and conditions: (i) NaH, chloroacetyl chloride **6**, THF, 6 h, rt; (ii) triethyl phosphite, 9 h, reflux; (iii) TMSBr (2 equiv), CH_3CN, microwave; (iv) TMSBr, DCM, overnight, rt; (v) 0.4 M-NaOH.

in binding to the hard Mg^{2+} cation in the DXR active site, and the heterocyclic moieties in compounds **8a–e** and **9a–e** were expected serve this function. Ester pro-drugs of fosmidomycin analogues have been shown to exhibit increased lipophilicity and absorption,[11–13] and the phosphonate esters **8a–e** might well provide similar advantages. Access to these compounds and the disodium salts **11a–e** of the corresponding phosphonic acids **9a–e** is outlined in Scheme 1.

Thus, acylation of the respective primary amines **5a–e** with chloroacetyl chloride **6** afforded the corresponding chloroacetamides **7a–e** in yields in excess of 70% and, generally, in sufficient purity to be used without further purification. The only exception was the 2-aminopyridine derivative **7a**, which was chromatographed prior to use. Phosphonation of the chloroacetamides **7a–e** was effected via the Arbuzov reaction using triethyl phosphite, and the diethyl phosphonates **8a–e** were readily isolated in moderate yields (48–67%). In each case, ^{1}H NMR analysis revealed disappearance of the chloromethylene singlet at ca. 4.2 ppm and the appearance of a methylene proton doublet at ca. 3 ppm, reflecting the distinctive coupling (J = ca. 21 Hz) to the adjacent ^{31}P nucleus. Since hydrolysis of the phosphonate esters **8a–e** to the corresponding acids **9a–e** is expected to occur in vivo,[12,14–16] the latter compounds were also required for in vitro enzyme-inhibition assays. Microwave-assisted hydrolysis of the esters in acetonitrile[17]—a method successfully used on similar compounds[9]—proved unsuccessful here. Consequently, the esters were simply stirred overnight with bromotrimethylsilane, followed by hydrolysis of the TMS-substituted intermediates **10a–e**, as described by McKenna et al.[18] This approach proved successful although extension of the reported[19] reaction time was necessary. (A ^{31}P NMR-based kinetics study has provided useful insights into the silylation mechanism.[20]) Titration of the TMS-substituted intermediates with aqueous sodium hydroxide afforded the disodium salts **11a–e**, two of which (**11a** and **11c**) required purification by reverse-phase semi-preparative HPLC.

2.2. Computer modelling

Simulated docking studies were undertaken to explore the binding affinity of the ligands **8a–e** and **9a–e** and the topology of the binding site. An in vacuo global minimum was located for each of the ligands following a systematic conformational search using Cerius^2.[21] Solvent-corrected, energy-minimised structures (including frequency calculations) were then obtained at the DFT level using Gaussian 03.[22] AutoDock version 4.0[23] was used for the docking studies, Discovery Studio Visualiser[24] to visualise the docked conformations and UCSF Chimera[25] to explore the active site. Preliminary in silico docking of the phosphonate esters **8a–e**, the phosphonic acids **9a–e** and the corresponding phosphonate dianions was explored using the active site (from which fosmidomycin **2** had been removed) in the crystal structure 1Q0L[26] of *Ec*DXR (which includes bound fosmidomycin **2** and NADPH). In order to simulate coordination to the divalent metal cation, Mn^{2+} was included in the model and positioned according to its location relative to fosmidomycin **2** and the coordinating ligands Asp150, Glu231 and Glu152 in the *Ec*DXR crystal structure 1ONP.[27] A charge of +2 was manually assigned to the manganese ion and the fosmidomycin was removed from the active site, as were the solvating water molecules. The active-site residues Ser186, Asn227, Lys228 and Glu231 were defined as flexible residues and simulated dockings were carried out with each of the ligands **8a–e** and **9a–e** as well as with DOXP **1**, fosmidomycin **2**, FR900098 **3** and the biosynthetic product, 2-*C*-methyl-D-erythritol 4-phosphate (MEP). Examination of docked conformations of each

of the ligands relative to fosmidomycin **2** and the proximal amino acid residues in the active site of the *Ec*DXR crystal structure 1Q0L[26] permitted potential hydrogen-bonding and Mn^{2+}-coordination distances to be determined. While the conformations of the majority of the docked ligands appeared to differ little from their minimum energy conformers, the solvent-corrected energies calculated for the docked ligands were all higher (by 63 ± 15 kcal · mol^{-1}) than their undocked conformers—the conformational energy cost of binding (Table 1).

In most cases, the ligands exhibited, unexpectedly, docking orientations opposite to that of fosmidomycin **2** (as illustrated in Fig. 2). In fact, in all of the crystal structures which include bound fosmidomycin, the hydroxamate moiety coordinates to the metal ion, close to NADPH, while the phosphonate group occupies a well-defined phosphonate-binding pocket[26,28]—an orientation which is essential for the conversion of DOXP to MEP. However, this does not preclude competitive 'reverse' binding of the natural substrate (DOXP) nor would it necessarily prevent a 'reverse'-bound ligand from acting as an inhibitor! Although the 'reverse'-binding mode is chemically feasible, Cheng and Oldfield have pointed out that the resultant four-membered ring would be more strained than the five-membered ring formed by 'normal' coordination of the hydroxamate moiety in fosmidomycin **2** to the metal cation.[29]

It was observed that a region adjacent to the phosphonate-binding pocket and lined by the residues, His257, Thr184, Glu152,

Table 1
Conformational binding cost,[a] and STD NMR binding, enzyme inhibition and IC_{50} data for ligands **8a–e** and **11a–e** using recombinant *Ec*DXR

Compound	Conformational binding cost[a]/kcal mol^{-1}	STD result	Enzyme inhibition[b,c]/%	IC_{50}/μM
8a	31.92	+	58.5	472
8b	54.45	+	11.7	1171
8c	67.10	+	28.9	730
8d	81.01	+	67.7	408
8e	66.08	+	21.6	1286
11a	84.47[d]	+	–[e]	–[e]
11b	45.02[d]	+	12.2	>1500
11c	44.79[d]	+	7.4	>1500
11d	47.06[d]	+	30.0	1027
11e	41.60[d]	+	16.6	>1500

[a] Energy between solvent-corrected, energy-minimised and docked conformers.
[b] At ligand concentration of 500 μM. At 0.3 μM, fosmidomycin **2** exhibits 99.3% inhibition of *Ec*DXR.
[c] Activity in the absence of inhibitor set at 100%.
[d] For the corresponding phosphonic acids **9a–e**.
[e] Anomalous result suggesting enzyme activation.

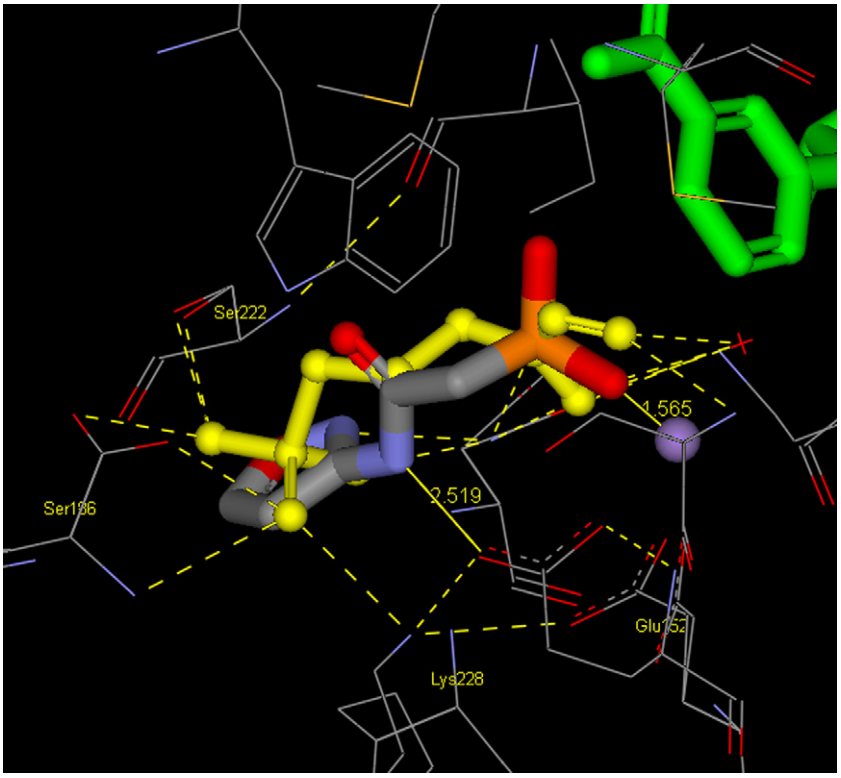

Figure 2. Docked conformation of ligand **9b** in the *Ec*DXR active site (1Q0L) with Mn^{2+} added, showing 'reverse' binding of the ligand relative to fosmidomycin **2**. Protein active-site residues are shown in wireframe coloured by atom type, NADPH as green sticks, Mn^{2+} as a purple sphere, and the ligand as sticks coloured by atom type. The crystal structure conformation of fosmidomycin **2** is shown in yellow ball-and-stick format. Hydrogen atoms have been omitted for clarity and hydrogen-bonding distances (in Å) are shown as yellow dashed lines.

Trp212 and the backbone atoms of Ser254 and Gly185, was regularly occupied by the heterocyclic moieties of the docked ligands (as illustrated in Fig. 3). Interestingly, some of the docking results for fosmidomycin **2** also indicate occupation of this region—an observation which could prove useful in the design of new inhibitors. In fact, this region may well be occupied by the highly active α-aryl phosphonates reported by Haemers et al.[30] and by Kurz et al.[31]

Little attention appears to have been given to placing the M^{2+} cation in the protein model[32] and to assigning a realistic charge to the metal centre. Typically, in docking studies which actually include the metal cation, Mg^{2+} has been used and has either been assigned a full +2 charge or the docking programme has been allowed to calculate a charge.[29,31] Although Silber et al.[33] and Perruchon et al.[34] state that Mg^{2+} is better parameterised than Mn^{2+} in AutoDock, a Gasteiger[35] charge of 0.00 is automatically assigned to either metal ion in AutoDock 4.0. Neither a charge of +2 nor 0 is likely to model the metal co-factor realistically in the presence of the surrounding, negatively charged, coordinating ligands. Consequently, in the present study, the Mg^{2+} cation, its coordinating residues (Asp149, Glu151 and Glu230), a water molecule and fosmidomycin **2**, were removed as a group from the crystal structure 2EGH,[28] and the group was energy-minimised, using a Hartree–Fock calculation.[22] This calculation afforded a charge of +1.058 on the Mg cation—a value consistent with significant dissipation the formal +2 charge by the coordinating ligands. The calculated Mulliken charges on all of the atoms in the energy-minimised group were transferred to the input files used by AutoDock and, when fosmidomycin **2** (with its Hartree–Fock calculated charges) was docked into the modified protein model, an increase in the number of correctly oriented dockings was observed. The importance of substrate or inhibitor binding to the metal cation[10,36] suggests that attention should be given to including a well-parameterised and accurately charged metal cation when carrying out docking studies on DXR.

2.3. Saturation Transfer Difference (STD) NMR experiments

STD NMR techniques have proved to be useful in qualitatively differentiating binding and non-binding ligands simultaneously in the presence of the enzyme.[37] Saturation of the protein is transferred to *bound* ligands resulting in an increase in their signal intensities; non-binding ligands are unaffected and subtraction of the reference spectrum from the saturation spectrum results in positive signals for the binding ligands alone. STD experiments were conducted, as described by Mayer and Meyer,[37] to screen the esters **8a–e** and the disodium salts **11a–e** for binding to *Ec*DXR (Table 1). The ligands all showed binding to *Ec*DXR, with minor, apparent anomalies being attributed to differences in T_1 relaxation times or distance-dependent[38] saturation transfer. Although the STD data provide an indication of protein–ligand-binding, the possibility of non-specific binding in regions other than the active site cannot be excluded.[39]

2.4. Enzyme-inhibition bioassays

Preliminary screening of the ability of the ligands **8a–e** and **11a–e** to inhibit *Ec*DXR was conducted using an enzyme assay based on the spectrophotometric measurement of the conversion of NADPH to NADP which occurs when DOXP is converted to MEP by DXR.[34,40,42] The ligands were tested at concentrations between 10 μM and 500 μM and the 500 μM data (Table 1) was used to assess their inhibition potential. While the % enzyme inhibition levels are relatively low and the IC_{50} concentrations correspondingly

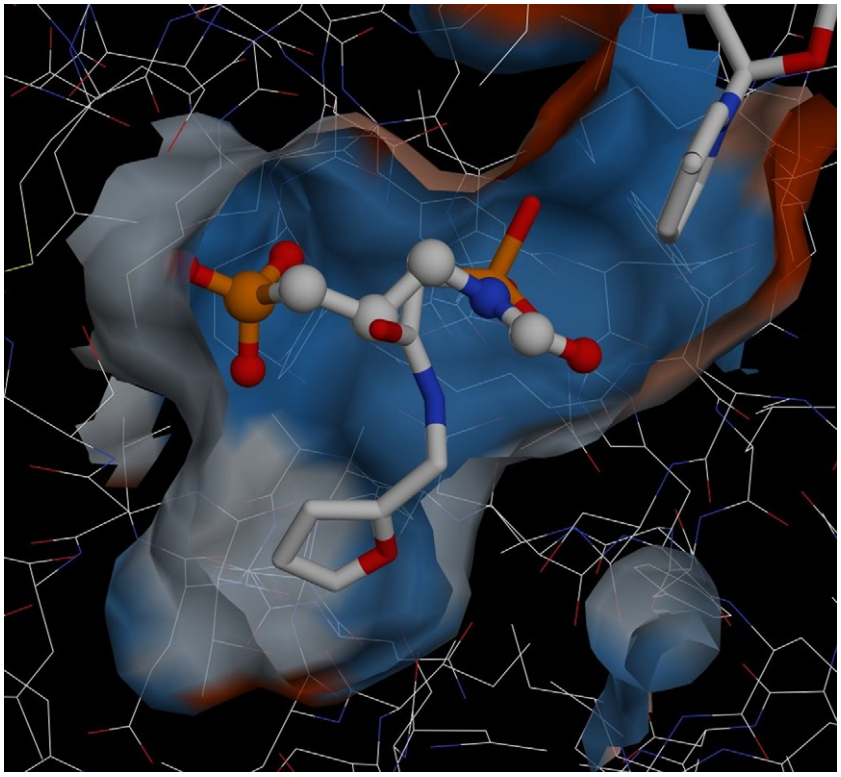

Figure 3. Docked conformation of ligand **9d** in *Ec*DXR (1Q0L) showing pocket in front of phosphonate-binding site occupied by the furan ring. The protein surface at 6.5 Å from fosmidomycin **2** is shown with 40% transparency, coloured to indicate hydrophilicity (blue) or hydrophobicity (orange) and clipped in front to expose the open pocket. Protein residues are shown in wireframe, coloured by atom type, the crystal structure fosmidomycin **2** in ball-and-stick format coloured by atom type and ligand **9d** and NADPH as sticks coloured by atom type. Hydrogen atoms have been omitted for clarity.

high, several of the ligands exhibit IC_{50} values in the micromolar range, the most active of these being the furan derivative **8d** (67.7% enzyme inhibition at 500 μM and IC_{50} = 408 μM). The data in Table 1 appear to reflect several structure–activity relationship patterns.

(i) The phosphonate esters **8** appear to exhibit significantly lower IC_{50} values than the corresponding phosphonic acid salts **11**—due, perhaps, to their more hydrophobic character and, hence, their relative preference for an enzymic rather than the aqueous environment. Perruchon et al.[34] explored the effect of extending the phosphonate ester groups and suggested that the negative effect of decreasing the charge on the phosphonate moiety is partly counteracted by the occupation of a nearby hydrophobic pocket by the alkyl ester groups.[34] This explanation could account for the higher inhibition shown by the phosphonate esters **8** compared to the phosphonic acid salts **11**.

(ii) Compound **8e**, which contains the bulkiest heteroaryl moiety, showed no inhibition at 500 μM, suggesting size constraints in the vicinity of the active site.

(iii) The fact that the furan derivatives **8d** and **11d** appear to be the most active ligands in their respective series—the former most active overall—may be due the flexibility provided by the furfuryl methylene group, which could increase the likelihood of the furan ring occupying the 'front' pocket. (In the other ligands, delocalisation of the amide nitrogen lone-pair into the heteroaryl ring would restrict their flexibility.) In fact, this possibility is supported by the observation that ligand **9d** docks most consistently (albeit in reversed orientation) with the furan ring occupying the 'front' pocket as illustrated in Figure 3; in this orientation the furan oxygen is suitably located to hydrogen-bond to the Ser151 or Glu152 residues.

3. Conclusions

The phosphonate esters **8a–e** and the corresponding phosphonic acid salts **11a–e** have been successfully synthesised and subjected to preliminary screening as DXR inhibitors using a combination of computer-modelling, STD NMR and enzyme-inhibition techniques. A number of the synthetic ligands have been shown to exhibit both enzyme-binding and enzyme-inhibition activity, while detailed investigation of the *Ec*DXR active site has permitted identification of an available pocket adjacent to the phosphonate-binding region, which is now being explored in the de novo design and development of a new series of potential ligands.

4. Experimental

4.1. Synthesis

The α-chloroamides **7a–e**, which are known, were prepared following a reported procedure.[41] The phosphonate esters **8a–e** and the corresponding phosphonic acid salts **11a–e**, which, with the exception of compound **11a**, are all new and were obtained as follows.

4.1.1. General procedure for the synthesis of the phosphonate esters 8a–e

The α-chloroamide starting material (**7a–e**) was placed in a dry, round-bottomed flask under N_2 and triethyl phosphite (5 equiv) was added through a septum. The mixture was refluxed (oil bath at 110 °C) for ca. 9 h. After cooling, hexane (20 mL) was added and the mixture stirred for ca. 20 min. The hexane was then decanted and stirring and decanting was repeated with three further aliquots of hexane. Evaporation of residual hexane and triethyl phosphite in vacuo afforded the desired ester **8**.

4.1.1.1. Diethyl 2-[(pyridin-2-yl)carbamoyl]ethylphosphonate 8a. As a dark brown oil (0.078 g, 12%) (Found: M^+, 272.091731. $C_{11}H_{17}N_2O_4P$ requires *M*, 272.092596); δ_H (600 MHz; $CDCl_3$) 1.35 (6H, t, *J* = 6.6 Hz, 2 × CH_3), 3.04 (2H, d, J_{H-P} = 21.0 Hz, CH_2P), 4.20 (4H, m, 2 × OCH_2), 7.04 (1H, m, ArH), 7.69 (1H, m, ArH), 8.13 (1H, d, *J* = 8.4 Hz, ArH), 8.28 (1H, d, *J* = 4.8 Hz, ArH), 8.96 (1H, s, NH); δ_C (150 MHz; $CDCl_3$) 16.4 (2 × CH_3), 36.9 (d, J_{C-P} = 129.0 Hz, CH_2P), 63.0 (d, J_{C-P} = 6 Hz, 2 × OCH_2), 114.0 (ArCH), 120.0 (5-ArCH), 138.3 (ArCH), 148.0 (ArCH), 151.0 (C-2), 162.7 (C=O); *m/z* 272 (M^+, 48%) and 94 (100).

4.1.1.2. Diethyl 2-[(isoxazol-3-yl)carbamoyl]ethylphosphonate 8b. As a dark brown oil which crystallised on standing (0.800 g, 48%), mp 60–66 °C (Found: M^+, 262.071312. $C_9H_{15}N_2O_5P$ requires *M*, 262.071860); δ_H (600 MHz; $CDCl_3$) 1.35 (6H, t, *J* = 7.2 Hz, 2 × CH_3), 3.10 (2H, d, J_{H-P} = 21.0 Hz, CH_2P), 4.20 (4H, m, 2 × OCH_2), 6.98 (1H, d, *J* = 1.8 Hz, ArCH), 8.25 (1H, d, *J* = 1.8 Hz, 5-ArCH), 9.95 (1H, s, NH); δ_C (150 MHz; $CDCl_3$) 16.3 (2 × CH_3), 36.2 (d, J_{C-P} = 130.5 Hz, CH_2P), 63.2 (d, J_{C-P} = 6 Hz, 2 × OCH_2), 99.3 (ArCH), 157.1 (C-3), 158.7 (ArCH), 162.5 (C=O); *m/z* 262 (M^+, 67%) and 179 (100).

4.1.1.3. Diethyl 2-[(1,3-thiazol-2-yl)carbamoyl]ethylphosphonate 8c. As a brown oil (1.04 g, 59%) (Found: M^+, 278.047217. $C_9H_{15}N_2O_4PS$ requires *M*, 278.049017); δ_H (600 MHz; $CDCl_3$) 1.32 (6H, t, *J* = 7.1 Hz, 2 × CH_3), 3.17 (2H, d, J_{H-P} = 21.6 Hz, CH_2P), 4.18 (4H, m, 2 × OCH_2), 6.96 (1H, d, *J* = 3.0 Hz, ArCH), 7.47 (1H, d, *J* = 3.0 Hz, ArCH); δ_C (150 MHz; $CDCl_3$) 16.2 (2 × CH_3), 35.6 (d, J_{C-P} = 131.3 Hz, CH_2P), 63.1 (d, J_{C-P} = 6 Hz, 2 × OCH_2), 113.6 (ArCH), 137.2 (ArCH), 158.5 (C-2), 162.4 (C=O); *m/z* 278 (M^+, 50%) and 179 (100).

4.1.1.4. Diethyl 2-[(furan-2-ylmethyl)carbamoyl]ethylphosphonate 8d. As a red-brown oil (1.09 g, 62%) (Found: M^+, 275.090706. $C_{11}H_{18}NO_5P$ requires *M*, 275.092261); δ_H (600 MHz; $CDCl_3$) 1.29 (6H, t, *J* = 7.2 Hz, 2 × CH_3) 2.85 (2H, d, J_{H-P} = 20.7 Hz, CH_2P), 4.90 (4H, m, 2 × OCH_2), 4.42 (2H, d, *J* = 5.7 Hz, CH_2N), 6.22 (1H, d, *J* = 3.0 Hz, 3-CH), 6.28 (1H, dd, *J* = 3.0 and 1.7 Hz, 4-CH), 7.17 (1H, s, NH), 7.31 (1H, d, *J* = 1.7 Hz, 5-CH); δ_C (150 MHz; $CDCl_3$) 16.2 (2 × CH_3), 35.0 (d, J_{C-P} = 129.0 Hz, CH_2P), 36.7 (CH_2NH), 62.7 (d, J_{C-P} = 6 Hz, 2 × OCH_2), 107.3 (ArCH), 110.3 (ArCH), 142.1 (ArCH), 151.0 (C-2), 163.8 (C=O); *m/z* 275 (M^+, 22%) and 96 (100).

4.1.1.5. Diethyl 2-[(5-acetyl-4-methyl-1,3-thiazol-2-yl)carbamoyl]ethyl-phosphonate 8e. As a yellow-brown solid (1.44 g, 67%), mp 151–154 °C [Found: $(M-1)^+$, 333.0667. $C_{12}H_{19}N_2O_5PS$ requires *M*−1, 333.0674); δ_H (600 MHz; $CDCl_3$) 1.38 (6H, t, *J* = 7.2 Hz, 2 × CH_3), 2.42 (3H, s, 4-CH_3), 2.49 (3H, s, CO·CH_3), 3.19 (2H, d, J_{H-P} = 22.2 Hz, CH_2P), 4.27 (4H, m, 2 × OCH_2); δ_C (150 MHz; $CDCl_3$) 16.3 (2 × CH_3CH_2), 18.2 ($CO.CH_3$), 30.2 (CH_3) 35.7 (d, J_{C-P} = 129.0 Hz, CH_2P), 63.6 (d, J_{C-P} = 7.5 Hz, 2 × OCH_2), 125.5 (ArC), 155.4 (ArC), 158.4 (ArC), 162.6 (NHC=O), 190.6 (CH_3C=O); *m/z* 333 (M−1, 100%).

4.1.2. General procedure for the hydrolysis of phosphonate esters to afford the phosphonic acid salts 11a–e[19]

The phosphonate ester **8** was dissolved in dry CH_2Cl_2 (3.5 mL) under N_2 and TMSBr (4 equiv) was added dropwise. The mixture was stirred overnight at room temperature and, after removal of the volatile material, in vacuo, the residue was dissolved in H_2O (2 mL) and the solution titrated with 0.40 M-NaOH to a pH of ca. 8.0. The aqueous solution was added to MeOH (ca. 200 mL) and

the resulting solution evaporated to dryness in vacuo. The crude product was purified by reverse-phase column chromatography on C_{18} cellulose, eluting with 1% NH_4OH in MeOH.

4.1.2.1. Disodium 2-[(pyridin-2-yl)carbamoyl]ethylphosphonate 11a. As a red-brown solid, which was further purified by HPLC (LUNA 10μ C_{18} column, 250 × 10.00 mm; elution with H_2O), (3 mg, 2.3% from HPLC) and which decomposes above 300 °C [Found: $(MH-Na_2)^+$, 215.0221. $C_7H_8N_2O_4P$ requires 215.0222]; δ_H (600 MHz; D_2O) 2.79 (2H, d, J_{H-P} = 18.6 Hz, CH_2P), 7.23 (1H, t, J = 6.0 Hz, ArH), 7.87 (2H, overlapping m, 2 × ArH), 8.31 (1H, d, J = 4.8 Hz, ArH); δ_C (150 MHz; D_2O) 40.1 (d, J_{C-P} = 109.5 Hz, CH_2P), 115.8 (d, ArCH), 120.8 (d, ArCH), 139.6 (d, ArCH), 147.7 (d, ArCH), 150.4 (s, 2-C), 171.9 (s, C=O); m/z 215 [$(MH-Na_2)^+$, 25%] and 218 (100).

4.1.2.2. Disodium 2-[(isoxazol-3-yl)carbamoyl]ethylphosphonate 11b. As a dark brown solid (0.438 g, quantitative yield), mp 283–285 °C (Found: MH^+, 250.9806. $C_5H_6N_2O_5PNa_2$ requires M+1, 250.9810); δ_H (600 MHz; D_2O) 2.79 (2H, d, J_{H-P} = 18.6 Hz, CH_2P), 6.80 (1H, d, J = 1.8 Hz, ArH), 8.51 (1H, d, J = 1.8 Hz, ArCH); δ_C (150 MHz; D_2O) 39.5 (d, J_{C-P} = 111.0 Hz, CH_2P), 99.1 (d, ArCH), 157.2 (s, ArC), 160.0 (d, ArCH), 170.8 (s, C=O); m/z 251 (MH^+, 87%) and 217 (100).

4.1.2.3. Disodium 2-[(1,3-thiazol-2-yl)carbamoyl]ethylphosphonate 11c. As a light brown solid (0.385 g, quantitative yield) which decomposes above 290 °C and which was further purified by reverse-phase chromatography [on C_{18} cellulose; elution with MeOH-0.1% aq NH_4OH] followed by HPLC (LUNA 10μ C_{18} column, 250 × 10.00 mm; elution with H_2O) (Found: MH^+, 266.9582. $C_5H_6N_2O_4SPNa_2$ requires M+1, 266.9581); δ_H (600 MHz; D_2O) 2.80 (2H, d, J_{H-P} = 18.6 Hz, CH_2P), 7.14 (1H, d, J = 3.6 Hz, ArH), 7.43 (1H, d, J = 3.6 Hz, ArH); δ_C (150 MHz; D_2O) 39.0 (d, J_{C-P} = 108.0 Hz, CH_2P), 114.0 (d, ArCH), 137.0 (d, ArC), 159.0 (s, ArC), 170.4 (s, C=O); m/z 267 (MH^+, 22%) and 223 (100).

4.1.2.4. Disodium 2-[(furan-2-ylmethyl)carbamoyl]ethylphosphonate 11d. As a brown solid (0.567 g, quantitative yield) which decomposes above 250 °C (Found: MH^+, 264.0010. $C_7H_9NO_5PNa_2$ requires M, 264.0014); δ_H (600 MHz; D_2O) 2.63 (2H, d, J_{H-P} = 19.2 Hz, CH_2P), 4.40 (2H, d, CH_2N), 6.36 (1H, d, J = 3.6 Hz, 3-CH), 6.44 (1H, dd, J = 3.6 and 1.8 Hz, 4-CH), 7.48 (1H, d, J = 1.8 Hz, 5-CH); δ_C (150 MHz; D_2O) 36.4 (t, CH_2N), 38.2 (d, J_{C-P} = 114.0 Hz, CH_2P), 107.1 (d, ArCH), 110.5 (d, ArCH), 142.5 (d, ArCH), 151.3 (s, 2-C), 172.1 (s, C=O); m/z 264 (MH^+, 3%) and 394 (100).

4.1.2.5. Disodium 2-[(5-acetyl-4-methyl-1,3-thiazol-2-yl)carbamoyl]ethylphos-phonate 11e. As a light brown solid (0.197 g, quantitative yield) which decomposes above 290 °C (Found: MH^+, 322.9856. $C_8H_{10}N_2O_5Na_2PS$ requires M+1, 322.9843); δ_H (600 MHz; D_2O) 2.59 (3H, s, CH_3), 2.61 (3H, s, $CO.CH_3$), 2.90 (2H, d, J_{H-P} = 18.6 Hz, CH_2P); δ_C (150 MHz; D_2O) 17.4 (q, CH_3) 29.3 (q, $CO{\cdot}CH_3$), 38.9 (d, J_{C-P} = 109.5 Hz, CH_2P), 125.7 (s, ArC), 156.3 (s, ArC), 161.1 (s, ArC), 170.5 (s, NHC=O), 195.7 (s, CH_3C=O); m/z 323 (MH^+, 100%).

4.2. Saturation Transfer Difference (STD) experiments[37]

*Ec*DXR was extracted and purified as described below. From a fraction containing 17.6 μM of *Ec*DXR in a 50 mM sodium phosphate buffer pH 7.0, 1.1 mL was removed and freeze-dried and then re-suspended in an equal volume of D_2O. An enzyme activity assay was performed on 100 μL of the re-suspended enzyme and the ligands were dissolved in the remaining 1 mL to give an approximate ratio of protein to ligand of 1:40. The actual concentrations of the 4 ligands in the enzyme solution were **11b** (748 μM), **11c** (748 μM), **11d** (969 μM) and **11e** (782 μM), and sodium 3-(trimethylsilyl)tetradeuteriopropanoate (TSP; 813 μM) was included as a standard. The STD assay was optimised in terms of the number of pre-saturation Gaussian pulses and the power level of the saturation pulse. Saturation of the protein was achieved using a train of 4 Gaussian bell-shaped pulses separated by a 1 ms delay at a power level of 40 dB. The frequency of the saturating on-resonance pulse was at 0.73 ppm and the off-resonance pulse at 20 ppm. Phase cycling between the on- and off-resonances was used to minimise the effects of slight changes in temperature or magnetic field homogeneity. No spin-lock filter was used. A 3-9-19 water suppression pulse was applied and 7168 scans were acquired. Spectra were subtracted and processed using Topspin software from Bruker.

4.3. Expression and purification of *Ec*DXR

*Ec*DXR was expressed and purified according to standard procedures.[40,42] In brief, XL-1 Blue competent cells were transformed with *Ec*DXR plasmid DNA. IPTG was used to induce expression of the recombinant *Ec*DXR gene. *Ec*DXR was then purified by a combination of Ni^{2+} affinity- and size exclusion-chromatography. The protein was stored at −20 °C in a sodium phosphate buffer of pH 7.

4.4. DXR inhibition assay[34,40,42]

Assays were conducted in a reaction mixture containing 100 mM Tris–HCl (pH 7.5), 1 mM $MgCl_2$, 0.3 mM NADPH and 0.3 mM DOXP in a total volume of 100 μL. Equal volumes of *Ec*DXR and ligand were incubated at 37 °C for 5 min; 100 μL of this enzyme–ligand mixture was then added to the rest of the assay components to make a total of 200 μL with a final *Ec*DXR concentration of 5 μg mL^{-1}. The decrease in absorbance at 340 nm due to the decreasing concentration of NADPH (ε_{NADPH} = 6.3×10^3 L mol^{-1} cm^{-1}) was followed for 10 min at 37 °C, relative to a blank lacking the DOXP substrate. For each ligand, enzyme activity in the absence of inhibitor was deemed to be 100% (i.e., 0% inhibition) and the % relative inhibition was determined in triplicate. Under these conditions, fosmidomycin **2** at 0.3 μM exhibited 99.3% inhibition.

Acknowledgements

The authors thank the Beit Trust for a bursary (to A.C.C), Rhodes University, LIFE*lab* and the South African Medical Research Council (MRC) for generous financial support, Jessica Goble for technical assistance with the expression and purification of *Ec*DXR and Professor Hassan Jomaa (Institute of Biochemistry, Academic Hospital Centre, Justus-Liebig-University) for the gift of the DXR plasmid.

Supplementary data

Supplementary data associated with this article can be found, in the online version, at doi:10.1016/j.bmc.2010.11.062.

References and notes

1. Areqawi, M.; Cibulskis, R.; Otten, M.; Williams, R.; Dye, C. *World Malaria Report; World Health Organisation: Geneva*, 2008; pp 1–125.
2. Müller, O.; Sié, A.; Meissner, P.; Schirmer, R. H.; Kouyaté, B. *Lancet* **2009**, *374*, 1419.
3. Trigg, P. I.; Kondrachine, A. V. The Current Global Malaria Situation. In *Malaria, Parasite Biology, Pathogenesis, and Protection*; Sherman, I. W., Ed.; American Society for Microbiology: Washington, DC, 1998; pp 11–22.
4. Rohmer, M.; Seemann, M.; Horbach, S.; Bringer-Meyer, S.; Sahm, H. *J. Am. Chem. Soc.* **1996**, *118*, 2564–2566.
5. Odom, A. R.; Van Voorhis, W. C. *Mol. Biochem. Parasitol.* **2010**, *170*, 108–111.

6. Jomaa, H.; Wiesner, J.; Sanderbrand, S.; Altincicek, B.; Weidemeyer, C.; Hintz, M.; Türbachova, I.; Eberl, M.; Zeidler, J.; Lichtenthaler, H. K.; Soldati, D.; Beck, E. *Science* **1999**, *285*, 1573–1576.
7. Singh, N.; Cheve, G.; Avery, M. A.; McCurdy, C. R. *Curr. Pharm. Des.* **2007**, *13*, 1161–1177.
8. Wiesner, J.; Borrmann, S.; Jomaa, H. *Parasitol. Res.* **2003**, *90*, S71–S76.
9. Mutorwa, M.; Salisu, S.; Blatch, G. L.; Kenyon, C.; Kaye, P. T. *Synth. Commun.* **2009**, *39*, 2723–2736.
10. Deng, L.; Sundriyal, S.; Rubio, V.; Shi, Z.; Song, Y. *J. Med. Chem.* **2009**, *52*, 6539–6542.
11. Ortmann, R.; Wiesner, J.; Reichenberg, A.; Henschker, D.; Beck, E.; Jomaa, H.; Schlitzer, M. *Bioorg. Med. Chem. Lett.* **2003**, *13*, 2163–2166.
12. Reichenberg, A.; Wiesner, J.; Weidemeyer, C.; Dreiseidler, E.; Sanderbrand, S.; Altincicek, B.; Beck, E.; Schlitzer, M.; Jomaa, H. *Bioorg. Med. Chem. Lett.* **2001**, *11*, 833–835.
13. Kurz, T.; Schlüter, K.; Kaula, U.; Bergmann, B.; Walter, R. D.; Geffken, D. *Bioorg. Med. Chem.* **2006**, *14*, 5121–5135.
14. Wiesner, J.; Ortmann, R.; Jomaa, H.; Schlitzer, M. *Arch. Pharm. (Weinheim)* **2007**, *340*, 667–669.
15. Krise, J. P.; Stella, V. J. *Adv. Drug Delivery Rev.* **1996**, *19*, 287–310.
16. Devreux, V.; Wiesner, J.; Jomaa, H.; Van der Eycken, J.; Van Calenbergh, S. *Bioorg. Med. Chem. Lett.* **2007**, *17*, 4920–4923.
17. Kumar, K. G. D.; Saenz, D.; Lokesh, G. L.; Natarajan, A. *Tetrahedron Lett.* **2006**, *47*, 6281–6284.
18. McKenna, C. E.; Higa, M. T.; Cheung, N. H.; McKenna, M. *Tetrahedron Lett.* **1977**, *18*, 155–158.
19. Giessmann, D.; Heidler, P.; Haemers, T.; Van Calenbergh, S.; Reichenberg, A.; Jomaa, H.; Weidemeyer, C.; Sanderbrand, S.; Wiesner, J.; Link, A. *Chem. Biodiversity* **2008**, *5*, 643–656.
20. Conibear, A. C.; Lobb, K. A.; Kaye, P. T. *Tetrahedron* **2010**, *66*, 8446–8449.
21. *Cerius*^{2}*, Version 4.10 L revision 05.0708*; Accelrys Inc.: Taipei, 1997.
22. Frisch, M. J.; Trucks, G. W.; Schlegel, H. B.; Scuseria, G. E.; Robb, M. A.; Cheeseman, J. R.; Montgomery, J. A., Jr., Vreven, T.; Kudin, K. N.; Burant, J. C.; Millam, J. M.; Iyengar, S. S.; Tomasi, J.; Barone, V.; Mennucci, B.; Cossi, M.; Scalmani, G.; Rega, N.; Petersson, G. A.; Nakatsuji, H.; Hada, M.; Ehara, M.; Toyota, K.; Fukuda, R.; Hasegawa, J.; Ishida, M.; Nakajima, T.; Honda, Y.; Kitao, O.; Nakai, H.; Klene, M.; Li, X.; Knox, J. E.; Hratchian, H. P.; Cross, J. B.; Bakken, V.; Adamo, C.; Jaramillo, J.; Gomperts, R.; Stratmann, R. E.; Yazyev, O.; Austin, A. J.; Cammi, R.; Pomelli, C.; Ochterski, J. W.; Ayala, P. Y.; Morokuma, K.; Voth, G. A.; Salvador, P.; Dannenberg, J. J.; Zakrzewski, V. G.; Dapprich, S.; Daniels, A. D.; Strain, M. C.; Farkas, O.; Malick, D. K.; Rabuck, A. D.; Raghavachari, K.; Foresman, J. B.; Ortiz, J. V.; Cui, Q.; Baboul, A. G.; Clifford, S.; Cioslowski, J.; Stefanov, B. B.; Liu, G.; Liashenko, A.; Piskorz, P.; Komaromi, I.; Martin, R. L.; Fox, D. J.; Keith, T.; Al-Laham, M. A.; Peng, C. Y.; Nanayakkara, A.; Challacombe, M.; Gill, P. M. W.; Johnson, B.; Chen, W.; Wong, M. W.; Gonzalez, C.; Pople, J. A. *GAUSSIAN 03, Revision E.01*; Gaussian, Inc.: Wallingford, CT, 2004.
23. Morris, G. M.; Goodsell, D. S.; Halliday, R. S.; Huey, R.; Hart, W. E.; Belew, R. K.; Olson, A. J. *J. Comput. Chem.* **1998**, *19*, 1639–1662.
24. *Discovery Studio Visualizer, Release 2.0*; Accelrys Software Inc.: San Diego, 2007.
25. Pettersen, E. F.; Goddard, T. D.; Huang, C. C.; Couch, G. S.; Greenblatt, D. M.; Meng, E. C.; Ferrin, T. E. *J. Comput. Chem.* **2004**, *25*, 1605–1612.
26. Mac Sweeney, A.; Lange, R.; Fernandes, R. P. M.; Schulz, H.; Dale, G. E.; Douangamath, A.; Proteau, P. J.; Oefner, C. *J. Mol. Biol.* **2005**, *345*, 115–127.
27. Steinbacher, S.; Kaiser, J.; Eisenreich, W.; Huber, R.; Bacher, A.; Rohdich, F. *J. Biol. Chem.* **2003**, *278*, 18401.
28. Yajima, S.; Hara, K.; Iino, D.; Sasaki, Y.; Kuzuyama, T.; Ohsawa, K.; Seto, H. *Acta Crystallogr., Sect. F: Struct. Biol. Cryst. Comm.* **2007**, *63*, 466–470.
29. Cheng, F.; Oldfield, E. *J. Med. Chem.* **2004**, *47*, 5149–5158.
30. Haemers, T.; Wiesner, J.; Busson, R.; Jomaa, H.; Van Calenbergh, S. *Eur. J. Org. Chem.* **2006**, *17*, 3856–3863; Haemers, T.; Wiesner, J.; Van Poecke, S.; Goeman, J.; Henschker, D.; Beck, E.; Jomaa, H.; Van Calenbergh, S. *Bioorg. Med. Chem. Lett.* **2006**, *16*, 1888–1891.
31. Kurz, T.; Schlueter, K.; Kaula, U.; Bergmann, B.; Walter, R. D.; Geffken, D. *Bioorg. Med. Chem.* **2006**, *14*, 5121–5135.
32. Singh, N.; Cheve, G.; Avery, M. A.; McCurdy, C. R. *J. Chem. Inf. Model.* **2006**, *46*, 1360–1370.
33. Silber, K.; Heidler, P.; Kurz, T.; Klebe, G. *J. Med. Chem.* **2005**, *48*, 3547–3563.
34. Perruchon, J.; Ortmann, R.; Altenkämper, M.; Silber, K.; Wiesner, J.; Jomaa, H.; Klebe, G.; Schlitzer, M. *ChemMedChem* **2008**, *3*, 1232–1241.
35. Gasteiger, J.; Marsili, M. *Tetrahedron* **1980**, *36*, 3219–3228.
36. Argyrou, A.; Blanchard, J. S. *Biochemistry* **2004**, *43*, 4375–4384.
37. Mayer, M.; Meyer, B. *Angew. Chem., Int. Ed.* **1999**, *38*, 1784–1788.
38. Yan, J.; Kline, A. D.; Mo, H.; Shapiro, M. J.; Zartler, E. R. *J. Magn. Reson.* **2003**, *163*, 270–276.
39. Ji, Z.; Yao, Z.; Liu, M. *Anal. Biochem.* **2009**, *385*, 380–382.
40. Kuzuyama, T.; Shimizu, T.; Takahashi, S.; Seto, H. *Tetrahedron Lett.* **1998**, *39*, 7913–7916.
41. Salisu, S. T. ATP Mimics as Glutamine Synthetase Inhibitors—an Exploratory Synthetic Study. PhD Thesis, Rhodes University, Grahamstown, 2008.
42. Kuntz, L.; Tritsch, D.; Grosdemange-Billiard, C.; Hemmerlin, A.; Willem, A.; Bach, T. J.; Rohmer, M. *Biochem. J.* **2005**, *386*, 127–135.